

# Higher Performance Visual Tracking with Dual-Modal Localization

Jinghao Zhou<sup>1,2</sup>, Bo Li<sup>2</sup>, Lei Qiao<sup>2</sup>, Peng Wang<sup>1</sup>  
 Weihao Gan<sup>2</sup>, Wei Wu<sup>2</sup>, Junjie Yan<sup>2</sup>, Wanli Ouyang<sup>3</sup>  
<sup>1</sup>Northwestern Polytechnical University  
<sup>2</sup>SenseTime Group Limited  
<sup>3</sup>University of Sydney

jensen.zhoujh@gmail.com, {libo,qiaolei,ganweihao}@sensetime.com,  
 peng.wang@nwpu.edu.cn, wanli.ouyang@sydney.edu.au

## Abstract

Visual Object Tracking (VOT) has synchronous needs for both robustness and accuracy. While most existing works fail to operate simultaneously on both, we investigate in this work the problem of conflicting performance between accuracy and robustness. We first conduct a systematic comparison among existing methods and analyze their restrictions in terms of accuracy and robustness. Specifically, 4 formulations—offline classification (OFC), offline regression (OFR), online classification (ONC), and online regression (ONR)—are considered, categorized by the existence of online update and the types of supervision signal. To account for the problem, we resort to the idea of ensemble and propose a dual-modal framework for target localization, consisting of robust localization suppressing distractors via ONR and the accurate localization attending to the target center precisely via OFC. To yield a final representation (i.e., bounding box), we propose a simple but effective score voting strategy to involve adjacent predictions such that the final representation does not commit to a single location. Operating beyond the real-time demand, our proposed method is further validated on 8 datasets—VOT2018, VOT2019, OTB2015, NFS, UAV123, LaSOT, TrackingNet, and GOT-10k, achieving state-of-the-art performance.

## 1. Introduction

Visual object tracking has synchronous needs for both robustness and accuracy. While the robustness stresses a tracker’s discriminability against distractors, the accuracy focuses on precise localization of the optimal point to further derive a high-fidelity representation. An ideal design of tracking algorithm requires successful handling for both needs. In the literature, online trackers [6, 5, 16, 2] conduct online learning during tracking such that the weight for dis-

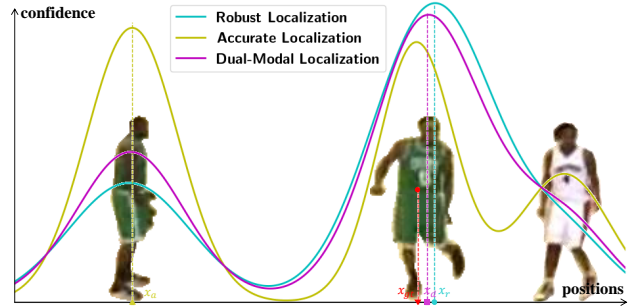


Figure 1. An 1D schematic illustration of our motivation.  $x_{gt}$  is the groundtruth. The prediction of accurate localization  $x_a$  is drifted severely but appears more shape-customized to derive boxes. The prediction of robust localization  $x_r$  handles well distinguishing distractors but fails to account for local details. The prediction of dual-modal localization  $x_d$  inherits both accuracy and robustness.

tinguishing target is adaptive to target deformation and object distraction. Though excelling in robustness by explicitly suppressing distractors, these approaches agonize over accurate tracking since regional center drift can be accumulated during online learning. On the contrary, offline trackers [1, 50, 24, 23] exclude online update and locate the target via matching the template to its most similar area. While these approaches lag in their robustness against distractors due to an intrinsic insufficiency of constructing clear class boundaries, they are good at voiding disruption of accumulated error thus are accurate in target center localization.

Considering that the requirements of robustness and accuracy can be contradictory, with the former insensitive to local details and robust in locating a rough target region while the latter sensitive to local details and accurate in determining optimal point for target representation, a divide-and-conquer strategy that solves them separately would be better than solving them integrally. Therefore, a dual-branch framework consisting of robust online tracking and accurate offline tracking arises naturally.

When robustness and accuracy are taken into further

consideration, the choice of supervision signals matters. For robust online tracking, a model trained with continuous Gaussian distribution can outperform that with a binary Bernoulli distribution, since target drift is more likely to happen when the binary Bernoulli distribution assigns all online predicted positives with equal significance. On the other hand, for accurate offline tracking, a Bernoulli distribution would be better with a more customized label assignment strategy [45, 49], especially in the presence of an extra anchor-scale dimension for anchor-based trackers [24, 23]. As shown in Figure 1, a dual-modal localization framework can inherit both accuracy and robustness, contributing to higher performance visual tracking.

Another important topic in visual tracking is the regression of target representation (i.e, the bounding box) upon the localized target center. Compared with that in static images, such in the field of object detection [34, 9, 37], box regression in tracking bear an intrinsic uncertainty of the target motion, deformation, and scale changes, etc. While recent studies [18, 5] resorts to overlap maximization of randomly drawn boxes via gradient descent, enabling a quick adaption to the uncertainty of target shape, such approach eludes accurate box regression with potentially ill-reached solutions due to random initial states and requires extra computational cost. To account for the uncertainty intrinsic in target representation for tracking, a simple but effective score voting strategy is proposed and directly involves adjacent predictions around the target center, improving the tracker’s capability for accurate tracking.

Our contributions can be summarised as three folds:

- We conduct a systematic comparison between 4 major existing approaches-ONR, ONC, OFR, and OFC in terms of accuracy and robustness. We further analyze the intrinsic restrictions of their design.
- We propose a dual-modal localization framework decoupling the task of target localization into robust localization via ONR and accurate localization via OFC.
- We propose a score voting strategy to account for the uncertainty in target representation, which is achieved by involving box predictions around the target center.

Together with the dual-modal localization framework and score voting strategy, our methods achieve state-of-the-art performance under major benchmarks while operating at a real-time speed at 41 Frame-Per-Second (FPS) on an NVIDIA Titan Xp GPU. Results on major benchmarks: VOT2018 [21], VOT2019 [22], OTB2015 [42], NFS [20], UAV123 [29], LaSOT [8], TrackingNet [30], and GOT-10k [17] verify the effectiveness of our method.

## 2. Related Work

The problem of visual tracking can be decomposed into two tasks: *target localization* where we first locate a rough

region of the target and *target representation* where we further regress a high-fidelity representation of it. Next, we shall discuss detailedly how the two tasks have been previously solved by the existing trackers.

**Target Localization.** Several recent studies [7, 11] formulate the problem of *target localization* as  $y^* = \arg \max_y s_\theta(y, x)$ , termed as *confidence-based regression*, where  $s_\theta : \mathcal{Y} \times \mathcal{X} \rightarrow \mathbb{R}$  predicts a scalar confidence score given an output-input pair  $(y_i, x_i)$ . To generate the localization heatmap convoluted by target-guided kernel formulated as  $s_\theta(y, x) = (w * \phi(x))(y)$ , the difference between the major trackers thus lies crucial in different paradigm in determining  $w$ . While offline trackers (e.g, siamese trackers [1, 24, 23, 25]) set  $w$  directly as the target feature  $\phi(z)$  and keep it fixed during tracking, online trackers (e.g, correlation-filter trackers [16, 6] and classifier-based trackers [32, 5, 2, 39], etc.) dynamically update  $w$  with online generated pseudo labels. Besides a categorization over tracker’s update strategy, the distribution of pseudo label generated by the function  $a : \mathcal{Y} \times \mathcal{Y} \rightarrow \mathbb{R}$  distinguishes the existing approaches into trackers based on classification and regression. For classification problem [1, 23, 32, 39], the pseudo label  $a(y, y_i) \in [0, 1]$  is binary (subject to Bernoulli distribution) and assigned often heuristically through Intersection-over-Union (IoU) between anchor and groundtruth boxes, with training loss  $l(a(y, y_i), s_\theta(y, x_i))$  set to cross-entropy loss. The pseudo label for regression problem [25, 2, 5, 16] is continuous between  $(0, 1)$  and often subject to a Gaussian distribution concentrated on target center with training loss being generative loss, like L2 or hinge loss. Following these two major categorizations of tracking algorithms, a combination of them results in 4 major formulations to solve tracking problem: online regression (ONR), online classification (ONC), offline regression (OFR), and offline classification (OFC).

**Dual-Branch Structure for Target Localization.** Our proposed dual-modal framework is a dual-branch structure, which has been previously studied by several works. [13, 12] decouples two branches respectively accounting for appearance and semantic features to represent the tracked object. [47, 36] consists of an online and an offline branch. While the offline branch is noise-free and allows no ambiguity, serving as guidance in selecting refined bounding boxes or masks, the online branch is rather discriminative against distractors. Our method resembles the last genres by decoupling into two localization models focusing respectively on robustness and accuracy. Different from them, which can be seen as a naive ensemble of two independent parts, our dual-modal framework achieves an end-to-end training and is validated to be optimal through a cross-over evaluation.

**Target Representation.** The target representation has been extensively studied in the field of visual tracking. Representations like bounding boxes [5, 24], masks [41], key-

form	method	update	distribution	A* $\uparrow$	R* $\downarrow$
ONR	DiMP [2]	$\checkmark$	Gaussian	0.582	<b>0.126</b>
ONC-1s	Det-MAML [39]	$\checkmark$	Bernoulli-1s	0.577	0.136
ONC-5s			Bernoulli-5s	0.587	0.133
OFR	SiamKPN [25]	$\times$	Gaussian	0.597	0.284
OFC-1s	SiamCAR [10]	$\times$	Bernoulli-1s	0.599	0.262
OFC-5s	SiamRPN++ [23]		Bernoulli-5s	<b>0.603</b>	0.254

Table 1. Comparison of 4 major formulations with their typical work, update strategy, label distribution, A (accuracy) and R (robustness). \* denotes the average results over multiple sets of hyper-parameters to ensure stability. See Appendix C for details.

points [28, 25], or their combination [43]) greatly boost the tracker’s performance in precise tracking. In this work, we focus on the discussion of the bounding box as representation. The traditional paradigm follows the idea of *direct regression* through  $b_\theta : \mathcal{X} \rightarrow \mathcal{Y}$  by directly adjusting randomly-drawn boxes [32] or preset anchor boxes [24, 23] around the coarsely localized target center. To tackle the commitment to a single state of *direct regression*, a recently-proposed study [5] performs a gradient-descending optimization strategy via IoU maximization. In this work, we propose a simple but effective score voting strategy to involve the adjacent locations around the target center to entail uncertainty in target representation.

### 3. Method

The problem of visual tracking has two synchronous needs for both accuracy and robustness. However, most of the trackers are unable to handle well the two requirements simultaneously given the intrinsic restrictions of their design. In this work, we first give a comparison and analysis of existing uni-modal framework for *target localization* in Section 3.1. We then introduce the proposed dual-modal localization framework in Section 3.2. Further, an effective score voting strategy for *target representation* is proposed in Section 3.3.

#### 3.1. Accuracy vs. Robustness

In this section, we first conduct a comparison among the major existing methods in terms of accuracy and robustness. Specifically, the Accuracy (A) and Robustness (R) proposed in VOT challenge [21] are chosen, where A computes the average overlap of tracked frames and R computes the average ratio of lost frames in a sequence. Specifically, OFC, OFR, ONC, and ONR, categorized by the existence of update strategy and the types of supervision signals, are evaluated. While the offline tracker does not need further qualification, for online trackers, we focus on the discussion of recently proposed state-of-the-art [2] in a meta-learning fashion, which leverages gradient-based strategy within an inner-loop to allow an end-to-end training of the backbones. The classification is supervised by Bernoulli distribution

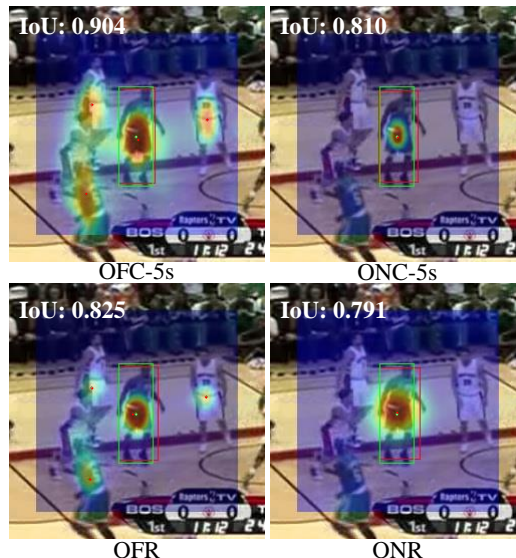


Figure 2. Accuracy vs. Robustness. Green box and point denote groundtruth box and center. Red box and points denote predicted box and local peaks. IoU between the prediction and groundtruth boxes are shown. Best viewed with color and zooming in.

while the regression is by Gaussian distribution. For a fair comparison, we unify the box branch same as in [23]. The results are shown in Table 1.  $\{-1, 5\}s$  denotes that the additional anchor scale dimension for classification is applied. The implementation details can be found later in Section 4. Next, we give a theoretical analysis of the pros and cons of each method in the context of their A and R.

**Online vs. Offline.** From the Table 1, we observe that one model often handles well one respect at a sacrifice of the other. *Specifically, we find that the online approaches excel at robustness while the offline approaches excel at accuracy.* We first give a theoretical analysis of how the conflicting performance under two metrics is caused. The superiority of robustness of online approaches stems from

- The online memory helps to store information about target historical deformation and potential distractors.
- The weight update helps the fast and discriminative parameterization via optimization under L2 loss.

On the contrary, offline approaches’ excellence at accuracy can be ascribed to

- The weight fixation avoids the ambiguity and accumulated error when assigning pseudo-labels.
- The weight fixation avoids generating target-centered prediction and allows more shape-customized prediction suitable for box regression.

For a visual demonstration, we provide the tracking results in Figure 2. Online approaches focus only on target while offline approaches have multiple peaks, validating the superiority of online approaches on robustness. Also, offline approaches tend to give larger center shift between the prediction and groundtruth, resulting in higher IoU scores. Next,

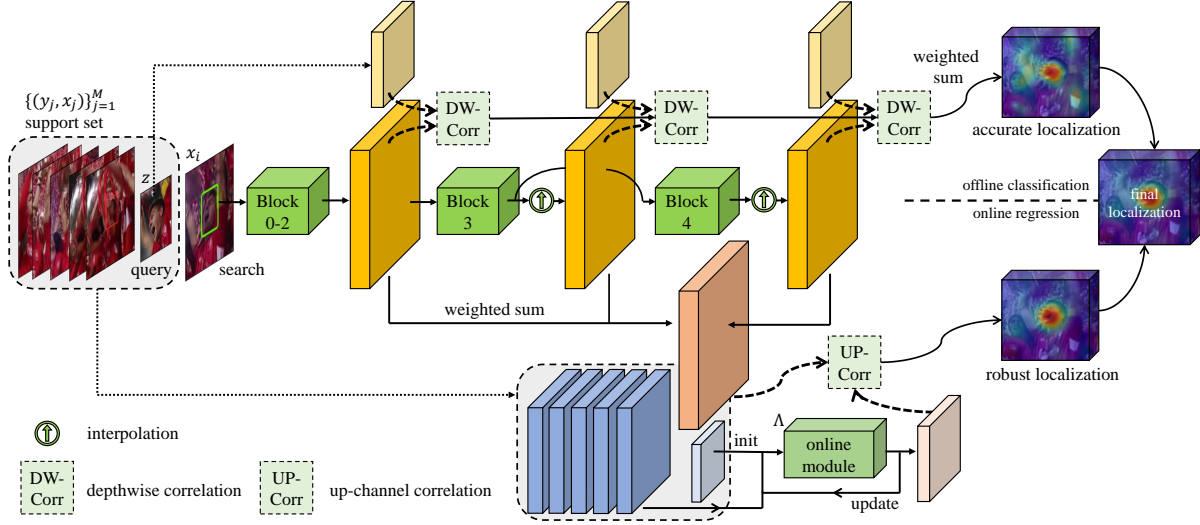


Figure 3. Architecture of proposed dual-modal localization framework. While OFC is applied for accurate localization, ONR is applied for robust localization. The final localization is weighted-sum of the two models. The derivation of bounding box is left out for succinctness.

we further investigate the influence of training labels on offline approaches and online approaches, focusing on the discussion of accuracy and robustness separately.

**OFC vs. OFR.** Comparing OFC-1s and OFR, we find that OFC-1s is slightly better in terms of accuracy. While the Gaussian distribution forces the adjacent region to have a lower score than the target center, the Bernoulli distribution allows multiple positives to be 1. Therefore, OFC-1s allows more uncertainty in deciding the optimal one to derive the final target representation. Beyond that, OFC-5s with an additional dimension of anchor scale further encodes representation information compared with single-scale regression or classification, thus achieves the optimal accuracy.

**ONC vs. ONR.** Comparing ONC- $\{1, 5s\}$  and ONR, ONR is slightly better than ONC in terms of robustness score. For robustness, we may expect the model to output a more target-centered prediction to avoid target drift. Therefore, the attribute of regression to suppress the surroundings around the target center can be beneficial in this regard. Further, compared with ONC, ONR allows more ambiguity in pseudo-label with wider peak region thus the surrounded pixels around target center remain certain probability to be considered as positive.

From the above analysis, we conclude that the advantages of specific formulation performing well under one metric also become the disadvantages of them performing well under the other, since uni-modal frameworks have their intrinsic restrictions of design. Intuitively, we consider a simple but effective ensemble of two diverse localization models that can handle well the separate needs of accuracy and robustness.

### 3.2. Dual-Modal Localization

In this section, a dual-modal localization framework decoupled into robust localization and accurate localization is proposed. Following the above experimental and theoretical analysis, we formulate robust localization into an ONR and accurate localization into an OFC. The two branches are trained independently with their own supervision signals and are directly fused to yield the final localization  $\hat{s}_\theta$  by weighted sum during inference, formulated as

$$\hat{s}_\theta(y, x_i) = \mu s_\theta^r(y, x_i) + (1 - \mu) s_\theta^a(y, x_i) \quad (1)$$

where  $\mu$  is a re-weighting hyper-parameter, stressing the significance of accurate and robust localization. Next, we shall detail how two localization models are implemented.

**Accurate Localization.** The accurate localization  $s_\theta^a$  applies OFC thus resembles anchor-based SiamRPN++ [23] by aggregating layer-wise correlation between first-frame template and the search region, formulate as

$$s_\theta^a(y, x_i) = \sum_{l=3}^5 \alpha^l (\phi_\theta^l(z) * \phi_\theta^l(x_i)) \quad (2)$$

where  $z$  is the template given by the first frame and  $\phi$  is the network parameterized by  $\theta$ . The correlation results of each layer are weighted by  $\alpha^l$ , which is jointly trained with the network. Specifically, the classification considers anchor an extra scale dimension besides spatial dimension for more accurate localization, yielding a heatmap for accurate localization  $s_\theta^a \in H \times W \times A$ . Detailed modifications and differences with SiamRPN++ can be found in Section 4.

**Robust Localization.** In contrast, the robust localization  $s_\theta^r$  applies ONR in a meta-learning fashion with inner-loop update. Out of the consideration of computation efficiency,

we conduct the aggregation in feature level thus only one fused weight is updated instead of a set of weights for each layer. The robust localization can be derived as

$$s_{\theta}^r(y, x_i) = \varphi * \sum_{l=3}^5 \beta^l \phi_{\theta}^l(x_i),$$

$$\text{where } \varphi = \Lambda\left(\sum_{l=3}^5 \beta^l \phi_{\theta}^l(z), \left\{\hat{a}(y, y_j), \sum_{l=3}^5 \beta^l \phi_{\theta}^l(x_j)\right\}_{j=1}^M; \rho\right) \quad (3)$$

$\varphi$  is an online updated and sequence-specific weight and  $\Lambda(\cdot; \rho)$  is an online module parameterized with  $\rho$ . For gradient-descent-based online module,  $\rho$  can be learned parameters such as learning rate, step size, or online generated pseudo label. The online module  $\Lambda$  takes fused feature of  $z$  as initial weight and are updated using a online-maintained feature support set  $\left\{\left(\hat{a}(y, y_j), \sum_{l=3}^5 \beta^l \phi_{\theta}^l(x_j)\right)\right\}_{j=1}^M$  as online training samples.  $\hat{a}(y, y_i)$  is online generated pseudo label and  $\beta^l$  is learned weight for layer  $l$  to aggregate the feature for fast online learning. By assigning Gaussian label for regression only on spatial scale, the heatmap for robust localization  $s_{\theta}^r \in H \times W$  can be obtained. Its weighted sum with offline classification score are conducted by a naive broadcasting over the missing dimension.

A complete architecture of our proposed dual-modal localization pipeline are shown in Figure 3. After obtaining the final localization, the state of target center to further regress target’s box representation is derived as  $y^* = \arg \max_y \hat{s}_{\theta}(y, x_i)$ .

### 3.3. Score Voting for Box Representation

The siamese trackers with Regional Proposal Network (RPN) [24, 23] obtain a final box representation by performing a direct regression upon the localized target center  $y^*$  as  $b^* = b_{\theta}(y^*, x_i)$  from the dense predictions  $b_{\theta}(y, x_i)$  over spatial scale, which is obtained similar to Equation 2 in an offline manner. However, the direct regression of box representation commits to only a single state  $y^*$ , ignoring potentially informative predictions on adjacent pixels. Inspired by [15], we acquire the final box representation  $b^*$  via a score voting strategy, where adjacent predictions around  $y^*$  from  $b_{\theta}(y, x_i)$  are leveraged to account for target’s multiple states and uncertainty in its shape, aspect ratio, and motion, etc. Our proposed score voting strategy can be formulated as

$$b^* = \frac{\int w(y, x_i) o_{\theta}(y, x_i) b_{\theta}(y, x_i) dy}{\int w(y, x_i) o_{\theta}(y, x_i) dy}, \quad (4)$$

$$\text{where } y \in \{y | \text{IoU}(b_{\theta}(y, x_i), b^*) > \epsilon\}$$

where  $o_{\theta}(y, x_i)$  is the IoU scores between the predicted box and groundtruth box via an additional IoU branch, the derivation of which can similarly resort to Equation 2. The IoU branch is trained end-to-end together with box branch

and dual-modal localization.  $w(y, x_i)$  is a penalized weight derived as

$$w(y, x_i) = \hat{s}_{\theta}(y, x_i) \odot e^{-(1-\text{IoU}(b_{\theta}(y, x_i), b^*))^2/\sigma} \quad (5)$$

where  $\hat{s}_{\theta}$  the final localization scores from Equation 1. The subsequent term represents a prior of Gaussian distribution of the real IoU between box representation at target center and adjacent box representations around.  $\odot$  denotes point-wise multiplication and  $\sigma$  is the variance term controlling the significance of the adjacent predictions and is set heuristically as a hyper-parameter. Compared with recently proposed [5], which applies a gradient-descent-based strategy to account for multiple states and uncertainty of target’s box representation, the obtaining of final box representation  $b^*$  via our score voting strategy is entirely fully-feedforward and introduce minimal extra computation cost to the current network. We provide a visualized demonstration to show the effectiveness of proposed score voting strategy in Appendix F.

## 4. Implementation Details

In this section, we showcase several implementation details of our approach. We include more detailed comments and the overall tracking algorithm in Appendix A.

**Online Approaches.** Following [2], we sample training data in a sequence-wise scheme with a support set  $Z$  and a query set  $Z'$ , each with 3 and 2 frames. The inner-loop of online approaches, including ONR and ONC is performed with  $Z$  under discriminative learning loss for fast convergence, where target mask and spatial weight are data-driven. The steepest gradient descent (SGD) with Gauss-Newton simplification is performed. For regression, the weight of the label generator (the coefficients of a radial basis function) is initialized as Gaussian and end-to-end trained with the network. For classification, the anchor boxes having IoU with predicted boxes higher than 0.8 and the one with the highest IoU are assigned as 1 while those lower than 0.3 as 0. The left ones are set to  $-1$  and ignored. For the outer-loop, the model is trained with  $Z'$  under hinge loss to avoid the dominance of easy negatives. The exact online learning formulation, loss function, and online tracking algorithm can be found in Appendix.

**Offline Approaches.** Following [50, 23], we conduct a pair-wise training scheme with negatives from randomly-sampled other videos<sup>1</sup>. While the training loss for classification is set to recently-proposed focal loss [26] to tackle class imbalance, the loss for training regression is a penalty-reduced variant of focal loss [48] to account for continuous values. The loss of negatives and positives samples are split

<sup>1</sup>If the offline and online approaches are jointly trained, we use the sequence-wise scheme instead. We take the averaged feature of  $Z$  as template and exclude negative pairs.

and normalized with each of their total amount such that background and foreground contribute equally to the total loss. The training label subject to Gaussian distribution for offline regression is centered at the target center with a variance set as a hyper-parameter according to the search window size, while the training label subject to Bernoulli distribution for offline classification is assigned using a modified version of recently-proposed ATSS [45]. More details can be found in Appendix.

**Network Architecture.** We use the original ResNet with interpolation instead of dilated ResNet for feature extraction (see Appendix B for details). Three  $1 \times 1$  convolution layers are attached to *block2* – 4 output reducing the dimension to 256. For offline approaches, an extra head is attached after depth-wise correlation reducing dimension from 256 to  $A$  (5 for OFC-5s, 1 for OFC-1s and OFR). The results are weighted sum over 3 layers. For online approaches, we first fuse features via weighted sum and have it up-channel correlated with the online updated weight  $\varphi$ , outputting the result with dimension  $A$  (5 for ONC-5s, 1 for ONC-1s and ONR). Figure 3 shows the overall architecture with OFC for accurate localization  $s_\theta^a$  and ONR for robust localization  $s_\theta^r$ . For target representation, the derivation of bounding boxes  $b_\theta$  resembles the offline approaches for target localization. A box head is attached for each of 3 layers after depth-wise correlation with the template reducing dimension from 256 to  $4 \times A$ . The IoU  $o_\theta$  for score voting is obtained by adding an extra slot to the box head instead of introducing an extra branch, yielding  $(\Delta cx, \Delta cy, \Delta w, \Delta h, o)$  for each anchor scale and overall output dimension being  $5 \times A$ . Note that for the dual-modal localization framework, the model’s output with smaller  $A$  is broadcast to the size of the larger one to obtain the representation result.

**Training Setup.** The training strategy is the same as [23]. The datasets we used for training include: ImageNet VID [35], Youtube-BB [33], COCO [27], LaSOT [8], and GOT-10k [17]. Our method is implemented in Python with PyTorch, and the experiments are conducted on a computer with NVIDIA GeForce GTX 1080ti GPUs. Following the discussions about loss of ONR and OFC above, together with losses for box offsets and IoU prediction, the total loss can derived as

$$L_{\text{total}} = \lambda_r L_r(s_\theta^r, y^r) + \lambda_a L_a(s_\theta^a, y^a) + \lambda_b L_b(b_\theta, y^b) + \lambda_o L_o(o_\theta, y^o) \quad (6)$$

where  $\lambda_r$ ,  $\lambda_a$ ,  $\lambda_b$ , and  $\lambda_o$  are re-weighting parameters and are set to 1, 10, 1.2, and 1.2 respectively.  $L_r$ ,  $L_a$ ,  $L_b$ , and  $L_o$  are focal loss, hinge loss, L1 loss, and binary cross-entropy (BCE) loss respectively.  $y^r$ ,  $y^a$ ,  $y^b$ , and  $y^o$  are training labels consisting of Gaussian heatmap, Bernoulli heatmap, box offsets, and box IoU respectively.

formulation	VOT2018			NUO323	
	A $\uparrow$	R $\downarrow$	EAO $\uparrow$	AUC $\uparrow$	NPr $\uparrow$
OFR	0.586	0.262	0.386	0.599	0.768
OFC-1s	0.601	0.225	0.394	0.601	0.769
OFC-5s	0.598	0.192	0.432	0.609	0.777
ONR	0.608	0.108	0.511	0.651	0.833
ONC-1s	0.578	0.089	0.488	0.640	0.814
ONC-5s	0.587	0.108	0.496	0.646	0.821
Ours	<b>0.612</b>	<b>0.084</b>	<b>0.540</b>	<b>0.665</b>	<b>0.844</b>

Table 2. Uni-Modal vs. Dual-Modal. The dual-modal localization framework with OFC-5s and ONR (bottom) achieves the top-performing results.

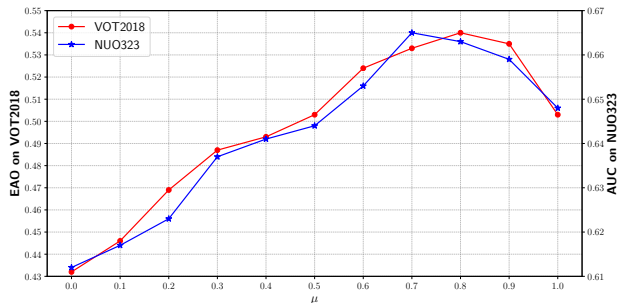


Figure 4. EAO on VOT2018 and AUC on NUO323 with varying fusion weight  $\mu$ .

## 5. Experiments

In this section, we first investigate the effectiveness of the proposed dual-modal localization framework and IoU voting strategy. Further, we evaluate our method on 8 benchmarks and compare the results with previous trackers.

### 5.1. Ablation Study

We perform extensive ablation studies to showcase the validity of our proposed method. The experiments are conducted on the dataset of VOT2018 and NUO323 (a combination of NFS100 (30fps), UAV123, and OTB100).

**Uni-Modal vs. Dual-Modal.** To illustrate the effectiveness of dual-modal architecture, we compare our method with the other uni-modal localization methods. For a fair comparison, all the other components (i.e., box branch, feature extraction, etc.) besides the localization part are kept identical. As illustrated in Table 2, online approaches generally demonstrate a stronger ability in terms of robustness according to R of VOT2018 dataset, while offline approaches have better accuracy with higher A. Among these formulations, ONR shows the best performance which indicates that robust localization is of overriding significance for good tracking. Our methods built upon ONR and OFC-5s reaches an EAO 0.540 on VOT2018 and an AUC 0.665 on NUO323, outperforming all 4 uni-modal localization methods by a large margin.

**Exhausting Dual-Modal Combinations.** As shown in Table 2, while online approaches excel at robust localiza-

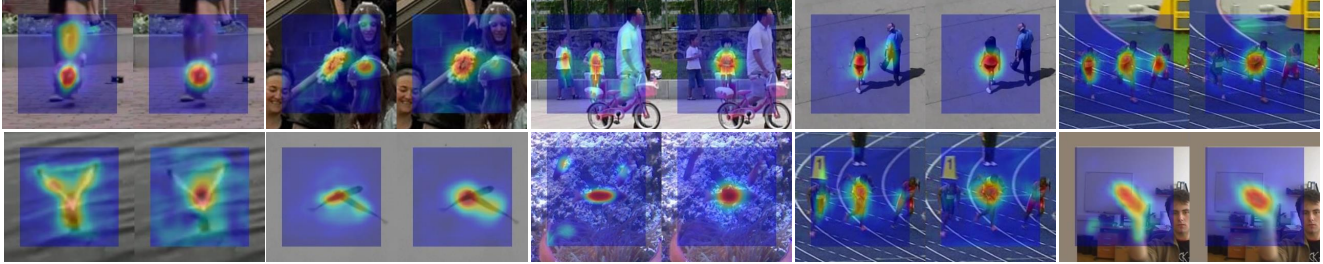


Figure 5. Visualization of the heatmap from two localization models. The left figure of each pair is heatmap of accurate localization, while the right one is the heatmap of robust localization. The output is maximized long the extra box scale dimension if with that.

offline	online	VOT2018			NUO323	
		A $\uparrow$	R $\downarrow$	EAO $\uparrow$	AUC $\uparrow$	NPr $\uparrow$
OFR	ONC-5s	0.604	0.122	0.512	0.648	0.823
OFC-1s		0.598	0.112	0.520	0.650	0.825
OFC-5s		0.601	0.098	0.533	0.656	0.837
OFR	ONC-1s	0.587	0.098	0.497	0.644	0.822
OFC-1s		0.596	0.112	0.498	0.648	0.829
OFC-5s		0.598	0.089	0.514	0.650	0.828
OFR	ONR	0.608	0.112	0.527	0.653	0.836
OFC-1s		0.592	0.112	0.523	0.656	0.840
OFC-5s		<b>0.612</b>	<b>0.084</b>	<b>0.540</b>	<b>0.665</b>	<b>0.844</b>

Table 3. Ablation study on other (offline + online) combinations for dual-modal framework.

score voting	VOT2018			NUO323	
	A $\uparrow$	R $\downarrow$	EAO $\uparrow$	AUC $\uparrow$	NPr $\uparrow$
w/o	<b>0.612</b>	0.084	0.540	0.665	0.844
w/	0.608	<b>0.080</b>	<b>0.564</b>	<b>0.671</b>	<b>0.859</b>

Table 4. Ablation study on the effectiveness of proposed score voting strategy for final box representation. w/ and w/o denotes voting strategy is and is not applied respectively.

tion, the offline approaches are good at accurate localization. Thus we further conduct a cross-over analysis by assigning different labels to the dual-modal framework, which consists of an online branch for robust localization and an offline branch localization. It can be observed from Table 3 that, online branch with a Gaussian label formulated as ONR generally yield high tracking performance. The combination of OFC-5s and ONC as accurate and robust localization respectively achieve a comparable result as well by achieving 0.642 of AUC on NUO323. Moreover, the offline branch with Bernoulli-5s as label tends to have higher accuracy than both Bernoulli-1s and Gaussian label, which validates the superiority of OFC-5s in accurate localization. From this above, our proposed dual-modal localization consisting of ONR and OFC is an optimal choice and outperform other combinations.

**Varying Fusion Weight.** With the obtained dual-modal framework consisting of ONR and OFC-5s, we investigate the effect of varying fusion weight  $\mu$  in terms of EAO on VOT2018 and AUC on NUO323. Results are shown in

Figure 4. We observe that the results are optimal around 0.7  $\sim$  0.8. The results also indicate that robust localization is more crucial for good tracking performance. We set  $\mu$  to 0.8 by default.

**Score Voting Strategy.** Next, we further illustrate the effectiveness of our proposed score voting strategy. From Table 4, with the introduction of score voting, the EAO of VOT2018 further rises from 0.54 to 0.564 and the AUC of NUO323 rises from 0.665 to 0.671. The consistent performance gain over two major benchmarks thus verifies the effectiveness of our proposed score voting strategy to account for uncertainty in the box representation.

**Visualization of Heatmaps.** To provide a demonstrative illustration of the superiority of each localization model, we showcase the heatmaps from the dual-modal framework over various sequences. As shown in Figure 5, the first row illustrates the superiority of robust localization with heatmaps from robust localization attending only to the target while those from accurate localization attending to other similar areas. In the scenarios of the presence of distractors, the robust localization can locate a rough region of the target more discriminatively thus greatly reduce the possibility of target drift. The second row of the figures illustrates the superiority of accurate localization over the robust one. While robust localization roughly locating the target, accurate localization is more customary to the target’s size thus more precise in locating the optimal point to further generate bounding boxes. Though other peaks occurred, the peak shape of accurate localization around the target is more dependent on the target’s original form. From these figures, the effectiveness of the framework of proposed dual-modal localization is verified given the complementary characteristics of two localization models.

## 5.2. Comparison with State-of-the-Arts

We compare our proposed tracker, termed as **DuML**, with the state-of-the-art approaches on the major benchmarks. Detailed results can be found in Appendix E.

**VOT2018 [21].** VOT2018 dataset consists of 60 challenging videos. The tracker’s overall performance is evaluated upon robustness and accuracy, defined using failure rate and

	UPDT [3]	SiamRPN ++[23]	ATOM [5]	DiMP [2]	DRDL [47]	Ocean [46]	FCOT [4]	RPT [28]	Ours
A $\uparrow$	0.536	0.600	0.590	0.597	<b>0.616</b>	0.592	0.600	<b>0.629</b>	<b>0.608</b>
R $\downarrow$	0.184	0.234	0.204	0.153	0.122	0.117	<b>0.108</b>	<b>0.103</b>	<b>0.080</b>
EAO $\uparrow$	0.378	0.414	0.401	0.440	0.481	0.489	<b>0.508</b>	<b>0.510</b>	<b>0.564</b>

Table 5. Results on VOT2018 challenge dataset [21] in terms of expected average overlap (EAO), robustness (R), and accuracy (A). Red, green and blue denote top-3 results.

	SiamM-ask[41]	SiamRPN ++[23]	ATOM [5]	STN [38]	Ocean [46]	DiMP [2]	DRNet [22]	RPT [28]	Ours
A $\uparrow$	0.594	0.580	<b>0.603</b>	0.589	0.594	0.594	<b>0.605</b>	<b>0.623</b>	<b>0.605</b>
R $\downarrow$	0.461	0.446	0.411	0.349	0.316	0.278	<b>0.261</b>	<b>0.186</b>	<b>0.176</b>
EAO $\uparrow$	0.287	0.292	0.301	0.314	0.350	0.379	<b>0.395</b>	<b>0.417</b>	<b>0.437</b>

Table 6. Results on VOT2019 challenge dataset [22] in terms of EAO, R, and A.

	MDNet[32]	ECO[6]	SiamRPN ++[23]	ATOM [5]	DiMP [2]	PrDiMP [7]	DRDL [47]	RPT [28]	Ours
OTB2015	67.8	69.1	<b>69.6</b>	66.9	68.4	69.5	<b>71.5</b>	<b>71.5</b>	<b>71.6</b>
NFS	42.2	46.6	-	58.4	<b>62.0</b>	<b>63.8</b>	-	-	<b>63.6</b>

Table 7. Results on OTB2015 and NFS (30fps) datasets [42, 20] in terms of overall AUC score.

IoU, and a comprehensive protocol EAO involves both two respects. We compare our methods with the state-of-the-art methods as shown in Table 5, resulting in an absolute gain on EAO from 0.510 to 0.564 with a 10.6% relative gain. Moreover, our tracker achieves the best robustness among all existing methods while maintaining a desirable accuracy. **VOT2019 [22]**. Compared with VOT2018, VOT2019 dataset includes more challenging sequences for evaluating the tracker’s robustness and accuracy. As shown in Table 6, our tracker consistently achieves a state-of-the-art result by outperforming the previously top tracker by 4.6% and resulting in an EAO of 0.437 and robustness of 0.176.

**OTB2015 [42]**. OTB2015 dataset contains a total amount of 100 sequences with motion, scale change, and illumination change, etc. The evaluation protocol is over precision plot and success plot (AUC). As shown in Table 7, we achieve a state-of-the-art performance with an AUC of 71.6 and a precision of 93.7.

**NFS (30fps) [20]**. The 30 fps version of dataset Need for Speed (NFS) resembles the evaluation protocol of OTB2015. With the fast motion of targets, along with challenging scenarios like distractors and scale change, NFS functions well for a comprehensive evaluation benchmark. As shown in Table 7, our tracker achieves an AUC score of 63.6 and a precision score of 77.4, indicating a desirable tracking capability.

**UAV123 [29]**. UAV123 dataset contains 123 sequences collected from a UAV perspective, which are practical in reality considering one major application of tracking algorithm is for UAVs’ purpose. As shown in Table 6, our tracker achieved an AUC score of 67.3 and a precision score of 88.4, with a large performance gain compared with the previous state-of-the-art trackers.

**LaSOT [8]** LaSOT is a challenging long-term tracking

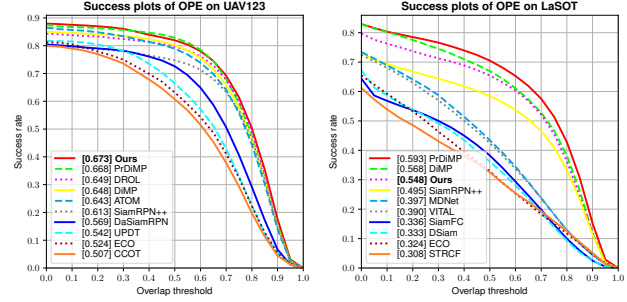


Figure 6. Results in terms of overall AUC score on UAV123 dataset [29] (left) and LaSOT dataset (right).

	SiamFC [1]	UPDT [3]	ATOM [5]	SPM [40]	SiamRPN ++[23]	DiMP [2]	DRDL [47]	SiamA- ttn[44]	Ours
AUC $\uparrow$	57.1	61.1	70.3	71.2	73.3	74.0	<b>74.6</b>	<b>75.2</b>	<b>74.7</b>
NPr $\uparrow$	66.6	70.2	77.1	77.8	80.0	<b>80.1</b>	<b>81.7</b>	<b>81.7</b>	<b>81.8</b>
Pr $\uparrow$	53.3	55.7	64.8	66.8	69.4	68.7	<b>70.8</b>	<b>71.5</b>	<b>70.9</b>

Table 8. Results on TrackingNet test set [30] in terms of precision (Pr), normalized precision (NPr), and success (AUC).

	SiamFC [1]	SiamRPN ++[23]	ATOM [5]	DMV [31]	DiMP [2]	Ocean [46]	FCOT [4]	Ours
SR $_{0.50}$ $\uparrow$	35.3	61.8	63.4	69.5	71.7	<b>72.1</b>	<b>76.3</b>	<b>72.8</b>
SR $_{0.75}$ $\uparrow$	9.8	32.9	40.2	<b>49.2</b>	<b>49.2</b>	48.7	<b>51.7</b>	<b>50.1</b>
AO $\uparrow$	34.8	51.8	55.6	60.1	<b>61.1</b>	<b>61.1</b>	<b>64.0</b>	<b>62.3</b>

Table 9. Results on GOT-10k test set [17] in terms of average overlap (AO), SR $_{0.75}$ , and SR $_{0.5}$ .

benchmark consisting of 280 sequences. The target can be out-of-frame and then reappear during tracking. From Table 6, our proposed method achieve comparable results compared with the top-performing methods, with an AUC score of 54.8 and a precision score of 56.3.

**TrackingNet [30]**. TrackingNet is a large-scale tracking benchmark, which consists of over 30k sequences in total and 511 sequences for testing without publicly available groundtruth. The results, shown in Table 8, demonstrates that our proposed method achieves state-of-the-art performance in terms of NPr precision and comparable performance in both AUC and precision.

**GOT-10k [17]**. GOT-10k is a recently-proposed large-scale dataset for both training and testing, with no overlap in object classes between training and testing. For GOT-10k test, we train our tracker by only using the GOT10k train split following its standard protocol. From Table 9, our proposed method achieves comparable results with the top methods with an AO of 62.7 and a SR $_{0.50}$  of 73.5.

## 6. Conclusion

In this work, we conduct a systematic investigation into accuracy and robustness for major 4 formulations existing in the tracking community. To account for the conflicting performance under accuracy and robustness, we analyze the underlying restrictions of each one’s design. Further, we resort to the idea of ensemble and propose a dual-modal local-

ization framework to account for separate needs for both robustness and accuracy, with the former solved by ONR and the latter by OFC. To account for the uncertainty in target representation, we propose a simple but effective score voting strategy to involve adjacent predicted boxes around the target center. The effectiveness of our method is validated among the major benchmarks with a large performance gain and a speed beyond the real-time requirement.

## References

- [1] Luca Bertinetto, Jack Valmadre, Joao F Henriques, Andrea Vedaldi, and Philip HS Torr. Fully-convolutional siamese networks for object tracking. In *European conference on computer vision*, pages 850–865. Springer, 2016. [1](#), [2](#), [8](#)
- [2] Goutam Bhat, Martin Danelljan, Luc Van Gool, and Radu Timofte. Learning discriminative model prediction for tracking. *arXiv preprint arXiv:1904.07220*, 2019. [1](#), [2](#), [3](#), [5](#), [8](#), [11](#), [12](#)
- [3] Goutam Bhat, Joakim Johnander, Martin Danelljan, Fahad Shahbaz Khan, and Michael Felsberg. Unveiling the power of deep tracking. In *Proceedings of the European Conference on Computer Vision (ECCV)*, September 2018. [8](#)
- [4] Yutao Cui, Cheng Jiang, Limin Wang, and Gangshan Wu. Fully convolutional online tracking, 2020. [8](#)
- [5] Martin Danelljan, Goutam Bhat, Fahad Shahbaz Khan, and Michael Felsberg. Atom: Accurate tracking by overlap maximization. In *Proceedings of the IEEE Conference on Computer Vision and Pattern Recognition*, pages 4660–4669, 2019. [1](#), [2](#), [3](#), [5](#), [8](#)
- [6] Martin Danelljan, Goutam Bhat, Fahad Shahbaz Khan, and Michael Felsberg. Eco: Efficient convolution operators for tracking. In *Proceedings of the IEEE conference on computer vision and pattern recognition*, pages 6638–6646, 2017. [1](#), [2](#), [8](#)
- [7] Martin Danelljan, Luc Van Gool, and Radu Timofte. Probabilistic regression for visual tracking. In *Proceedings of the IEEE/CVF Conference on Computer Vision and Pattern Recognition*, pages 7183–7192, 2020. [2](#), [8](#)
- [8] Heng Fan, Liting Lin, Fan Yang, Peng Chu, Ge Deng, Sijia Yu, Hexin Bai, Yong Xu, Chunyuan Liao, and Haibin Ling. Lasot: A high-quality benchmark for large-scale single object tracking. In *Proceedings of the IEEE conference on computer vision and pattern recognition*, pages 5374–5383, 2019. [2](#), [6](#), [8](#), [12](#)
- [9] Ross Girshick. Fast r-cnn. In *Proceedings of the IEEE international conference on computer vision*, pages 1440–1448, 2015. [2](#)
- [10] Dongyan Guo, Jun Wang, Ying Cui, Zhenhua Wang, and Shengyong Chen. Siamcar: Siamese fully convolutional classification and regression for visual tracking. In *Proceedings of the IEEE/CVF Conference on Computer Vision and Pattern Recognition*, pages 6269–6277, 2020. [3](#)
- [11] Fredrik K Gustafsson, Martin Danelljan, Goutam Bhat, and Thomas B Schön. Energy-based models for deep probabilistic regression. In *Proceedings of the European Conference on Computer Vision (ECCV)*, 2020. [2](#)
- [12] Anfeng He, Chong Luo, Xinmei Tian, and Wenjun Zeng. Towards a better match in siamese network based visual object tracker. In *Proceedings of the European Conference on Computer Vision (ECCV)*, pages 0–0, 2018. [2](#)
- [13] Anfeng He, Chong Luo, Xinmei Tian, and Wenjun Zeng. A twofold siamese network for real-time object tracking. In *Proceedings of the IEEE Conference on Computer Vision and Pattern Recognition*, pages 4834–4843, 2018. [2](#)
- [14] Kaiming He, Xiangyu Zhang, Shaoqing Ren, and Jian Sun. Deep residual learning for image recognition. In *Proceedings of the IEEE conference on computer vision and pattern recognition*, pages 770–778, 2016. [11](#)
- [15] Yihui He, Chenchen Zhu, Jianren Wang, Marios Savvides, and Xiangyu Zhang. Bounding box regression with uncertainty for accurate object detection. In *Proceedings of the IEEE Conference on Computer Vision and Pattern Recognition*, pages 2888–2897, 2019. [5](#)
- [16] João F Henriques, Rui Caseiro, Pedro Martins, and Jorge Batista. High-speed tracking with kernelized correlation filters. *IEEE transactions on pattern analysis and machine intelligence*, 37(3):583–596, 2014. [1](#), [2](#)
- [17] Lianghua Huang, Xin Zhao, and Kaiqi Huang. Got-10k: A large high-diversity benchmark for generic object tracking in the wild. *IEEE Transactions on Pattern Analysis and Machine Intelligence*, 2019. [2](#), [6](#), [8](#), [12](#)
- [18] Borui Jiang, Ruixuan Luo, Jiayuan Mao, Tete Xiao, and Yunying Jiang. Acquisition of localization confidence for accurate object detection. In *Proceedings of the European Conference on Computer Vision (ECCV)*, pages 784–799, 2018. [2](#)
- [19] Borui Jiang, Ruixuan Luo, Jiayuan Mao, Tete Xiao, and Yunying Jiang. Acquisition of localization confidence for accurate object detection. In *Proceedings of the European Conference on Computer Vision (ECCV)*, pages 784–799, 2018. [11](#)
- [20] Hamed Kiani Galoogahi, Ashton Fagg, Chen Huang, Deva Ramanan, and Simon Lucey. Need for speed: A benchmark for higher frame rate object tracking. In *Proceedings of the IEEE International Conference on Computer Vision*, pages 1125–1134, 2017. [2](#), [8](#), [12](#)
- [21] Matej Kristan, Ales Leonardis, Jiri Matas, Michael Felsberg, Roman Pflugfelder, Luka Cehovin Zajc, Tomas Vojir, Goutam Bhat, Alan Lukezic, Abdelrahman Eldesokey, et al. The sixth visual object tracking vot2018 challenge results. In *Proceedings of the European Conference on Computer Vision (ECCV)*, pages 0–0, 2018. [2](#), [3](#), [7](#), [8](#)
- [22] Matej Kristan, Jiri Matas, Ales Leonardis, Michael Felsberg, Roman Pflugfelder, Joni-Kristian Kamarainen, Luka Cehovin Zajc, Ondrej Drbohlav, Alan Lukezic, Amanda Berg, et al. The seventh visual object tracking vot2019 challenge results. In *Proceedings of the IEEE International Conference on Computer Vision Workshops*, pages 0–0, 2019. [2](#), [8](#)
- [23] Bo Li, Wei Wu, Qiang Wang, Fangyi Zhang, Junliang Xing, and Junjie Yan. Siamrpn++: Evolution of siamese visual tracking with very deep networks. In *Proceedings of the IEEE Conference on Computer Vision and Pattern Recognition*, pages 4282–4291, 2019. [1](#), [2](#), [3](#), [4](#), [5](#), [6](#), [8](#), [11](#), [12](#)
- [24] Bo Li, Wei Wu, Zheng Zhu, Junjie Yan, and Xiaolin Hu. High performance visual tracking with siamese region pro-

- positional network. *IEEE Conference on Computer Vision and Pattern Recognition (CVPR)*, 2018. 1, 2, 3, 5, 11, 12
- [25] Qiang Li, Zekui Qin, Wenbo Zhang, and Wen Zheng. Siamese keypoint prediction network for visual object tracking. *arXiv preprint arXiv:2006.04078*, 2020. 2, 3
- [26] Tsung-Yi Lin, Priya Goyal, Ross Girshick, Kaiming He, and Piotr Dollár. Focal loss for dense object detection. In *Proceedings of the IEEE international conference on computer vision*, pages 2980–2988, 2017. 5, 11
- [27] Tsung-Yi Lin, Michael Maire, Serge Belongie, James Hays, Pietro Perona, Deva Ramanan, Piotr Dollár, and C Lawrence Zitnick. Microsoft coco: Common objects in context. In *European conference on computer vision*, pages 740–755. Springer, 2014. 6, 12
- [28] Ziang Ma, Linyuan Wang, Haitao Zhang, Wei Lu, and Jun Yin. Rpt: Learning point set representation for siamese visual tracking. *arXiv preprint arXiv:2008.03467*, 2020. 3, 8
- [29] Matthias Mueller, Neil Smith, and Bernard Ghanem. A benchmark and simulator for uav tracking. In *European conference on computer vision*, pages 445–461. Springer, 2016. 2, 8, 12
- [30] Matthias Muller, Adel Bibi, Silvio Giancola, Salman Alsubaihi, and Bernard Ghanem. Trackingnet: A large-scale dataset and benchmark for object tracking in the wild. In *Proceedings of the European Conference on Computer Vision (ECCV)*, pages 300–317, 2018. 2, 8
- [31] Gunhee Nam, Seoung Wug Oh, Joon-Young Lee, and Seon Joo Kim. Dmv: Visual object tracking via part-level dense memory and voting-based retrieval, 2020. 8
- [32] Hyeonseob Nam and Bohyung Han. Learning multi-domain convolutional neural networks for visual tracking. In *Proceedings of the IEEE conference on computer vision and pattern recognition*, pages 4293–4302, 2016. 2, 3, 8
- [33] Esteban Real, Jonathon Shlens, Stefano Mazzocchi, Xin Pan, and Vincent Vanhoucke. Youtube-boundingboxes: A large high-precision human-annotated data set for object detection in video. In *proceedings of the IEEE Conference on Computer Vision and Pattern Recognition*, pages 5296–5305, 2017. 6, 12
- [34] Joseph Redmon, Santosh Divvala, Ross Girshick, and Ali Farhadi. You only look once: Unified, real-time object detection. In *Proceedings of the IEEE conference on computer vision and pattern recognition*, pages 779–788, 2016. 2
- [35] Olga Russakovsky, Jia Deng, Hao Su, Jonathan Krause, Sanjeev Satheesh, Sean Ma, Zhiheng Huang, Andrej Karpathy, Aditya Khosla, Michael Bernstein, et al. Imagenet large scale visual recognition challenge. *International journal of computer vision*, 115(3):211–252, 2015. 6, 12
- [36] Hao Shen, Defu Lin, Tao Song, and Guangyu Gao. Anti-distractors: two-branch siamese tracker with both static and dynamic filters for object tracking. *Multimedia Systems*, 26(6):631–641, 2020. 2
- [37] Zhi Tian, Chunhua Shen, Hao Chen, and Tong He. Fcos: Fully convolutional one-stage object detection. In *Proceedings of the IEEE international conference on computer vision*, pages 9627–9636, 2019. 2
- [38] A. S. Tripathi, Martin Danelljan, L. Gool, and R. Timofte. Tracking the known and the unknown by leveraging semantic information. In *BMVC*, 2019. 8
- [39] Guangting Wang, Chong Luo, Xiaoyan Sun, Zhiwei Xiong, and Wenjun Zeng. Tracking by instance detection: A meta-learning approach. In *Proceedings of the IEEE/CVF Conference on Computer Vision and Pattern Recognition*, pages 6288–6297, 2020. 2, 3
- [40] Guangting Wang, Chong Luo, Zhiwei Xiong, and Wenjun Zeng. Spm-tracker: Series-parallel matching for real-time visual object tracking. In *Proceedings of the IEEE Conference on Computer Vision and Pattern Recognition*, pages 3643–3652, 2019. 8
- [41] Qiang Wang, Li Zhang, Luca Bertinetto, Weiming Hu, and Philip HS Torr. Fast online object tracking and segmentation: A unifying approach. In *Proceedings of the IEEE conference on computer vision and pattern recognition*, pages 1328–1338, 2019. 2, 8
- [42] Y. Wu, J. Lim, and M. Yang. Object tracking benchmark. *IEEE Transactions on Pattern Analysis and Machine Intelligence*, 37(9):1834–1848, 2015. 2, 8, 12
- [43] Bin Yan, Dong Wang, Huchuan Lu, and Xiaoyun Yang. Alpha-refine: Boosting tracking performance by precise bounding box estimation. *arXiv preprint arXiv:2007.02024*, 2020. 3
- [44] Yuechen Yu, Yilei Xiong, Weilin Huang, and Matthew R. Scott. Deformable siamese attention networks for visual object tracking. In *Proceedings of the IEEE/CVF Conference on Computer Vision and Pattern Recognition (CVPR)*, June 2020. 8
- [45] Shifeng Zhang, Cheng Chi, Yongqiang Yao, Zhen Lei, and Stan Z Li. Bridging the gap between anchor-based and anchor-free detection via adaptive training sample selection. In *Proceedings of the IEEE/CVF Conference on Computer Vision and Pattern Recognition*, pages 9759–9768, 2020. 2, 6, 11
- [46] Zhipeng Zhang, Houwen Peng, Jianlong Fu, Bing Li, and Weiming Hu. Ocean: Object-aware anchor-free tracking. In *The IEEE Conference on European Conference on Computer Vision (ECCV)*, August 2020. 8
- [47] Jinghao Zhou, Peng Wang, and Haoyang Sun. Discriminative and robust online learning for siamese visual tracking. In *AAAI*, pages 13017–13024, 2020. 2, 8
- [48] Xingyi Zhou, Dequan Wang, and Philipp Krähenbühl. Objects as points. *arXiv preprint arXiv:1904.07850*, 2019. 5, 11
- [49] Benjin Zhu, Jianfeng Wang, Zhengkai Jiang, Fuhang Zong, Songtao Liu, Zeming Li, and Jian Sun. Autoassign: Differentiable label assignment for dense object detection. *arXiv preprint arXiv:2007.03496*, 2020. 2
- [50] Zheng Zhu, Qiang Wang, Bo Li, Wei Wu, Junjie Yan, and Weiming Hu. Distractor-aware siamese networks for visual object tracking. In *Proceedings of the European Conference on Computer Vision (ECCV)*, pages 101–117, 2018. 1, 5

## A. Implementation Details

**Online Approaches (ONC & ONR) with Discriminative Learning Loss and Steepest Gradient Descent [2].** We follow the same formulation and update strategy for online learning as DiMP [2]. Specifically, the inner-loop is trained under the least-square error with the residue defined as

$$r(p, c) = v_c \cdot (m_c p + (1 - m_c) \max(0, p) - y_c) \quad (7)$$

where  $p$  is the prediction and  $c$  is the target center.  $v_c$ ,  $m_c$ , and  $y_c$  are offline trained as the coefficients of a set of triangular basis functions. Further, we use steepest gradient descent, which scales the step length with its Hessian matrix  $Q$  and further the inner product of Jacobian vector as  $Q = J^T J$ , formulated as

$$\theta^{(i+1)} = \theta^{(i)} - \frac{\nabla L(\theta^{(i)})^T \nabla L(\theta^{(i)})}{\nabla L(\theta^{(i)})^T Q \nabla L(\theta^{(i)})} \nabla L(\theta^{(i)}) \quad (8)$$

where  $i$  denotes the number of iterations of stepwise optimization. We initialize the parameter  $\theta^{(0)}$  with template feature adaptively pooled (instead of using precise RoI pooling [19]) to the kernel size  $5 \times 5$ .

**Offline Classification (OFC) with Focal Loss [26] and ATSS [45].** To further alleviate the problem of class imbalance, we utilized focal loss for training OFC. As for label assignment, [23] assigns the positive and negative according to the computed IoU between anchor boxes and groundtruth. The recently-proposed ATSS [45] assigns the positive and negative according to the pre-computed statistics which bridges the gap between anchor-based and anchor-free detectors. The original ATSS computes the mean and variance of boxes whose center is closest to the center of groundtruth based on L2 distance. We denote it as  $ATSS_{Min.L2}$ . In practice, we compute statistics of top-15 anchor boxes for OFC-5s and top-11 anchor boxes for OFC-1s having the highest IoU with the groundtruth to assign the positive and negative anchors, which yield higher performance. We denote it as  $ATSS_{Max.IoU}$ . Our modifications and implementations for OFC serve as a stronger baseline compared to SiamRPN++, shown in Table 10.

form	label assignment	loss	VOT2018		
			Acc	R	EAO
OFC-5s	IoU	CE	0.601	0.201	0.414
	IoU	FC	0.608	0.215	0.419
	$ATSS_{Min.L2}$	FC	0.596	0.201	0.425
	$ATSS_{Max.IoU}$	FC	0.598	0.192	0.432
OFC-1s	$ATSS_{Min.L2}$	FC	0.604	0.231	0.386
	$ATSS_{Max.IoU}$	FC	0.601	0.225	0.394
OFR	Gaussian	$FC_{RG}$	0.594	0.276	0.375
	Gaussian	$FC_{PR}$	0.586	0.262	0.386

Table 10. Ablation study on different modifications for OFC and OFR.

## Offline Regression (OFR) with Continuous Focal Loss.

We consider the continuous variants of focal loss to train the offline regression. Specifically, we consider the penalty-reduced focal loss [48], denoted as  $FC_{PR}$ , where the pixels at the center of Gaussian as positive examples while the others as negatives whose loss is reduced corresponding to its continuous labels, formulated as

$$L = -\frac{1}{N} \sum_y \begin{cases} (1 - P_y)^\alpha \log(P_y) & \text{if } Y_y = 1 \\ (1 - Y_y)^\beta P_y^\alpha \log(1 - P_y) & \text{otherwise} \end{cases} \quad (9)$$

where  $\alpha$  and  $\beta$  are hyper-parameters. While the continuous value can be regressed, the local optima of this loss is not the groundtruth label. To tackle this problem, we have tried another similar loss, denoted as regressive focal loss, with  $P = Y$  holds true at the optimal point. The  $FC_{RG}$  can be formulated as

$$L = -\frac{1}{N} \sum_y -Y_y^\beta (Y_y - P_y)^\alpha \log(P_y) \quad (10)$$

where  $\alpha \in \{2n \mid n \in N^+\}$  and  $\beta$  are hyper-parameters. We set  $\alpha$  to 2 and  $\beta$  to 4 for both losses. We observe that  $FC_{PR}$  works better in practice, shown in 10. We use  $FC_{PR}$  in all our experiments.

**Tracking Algorithm.** During tracking, a support set with memory size  $M = 50$  is maintained for ONR to record historical glances of the target with a fixed space of augmented initial frames. For initialization, the weight is optimized for 10 iterations with an augmented support set obtained from the first frame. For online tracking, the update is conducted with a learning rate of 0.1 and 2 iterations every 20 frame, or a learning rate of 0.2 and 1 iteration once the possible distractors are detected. If the target is lost, we discard that frame. We recommend the readers to refer to [2] for more technical details. After fusing the heatmap of ONR and OFC, we apply the same post-processing process as [24] (i.e., cosine window, box temporal smoothing, etc.) We recommend the readers to refer to [24] for more details. The search region is set to  $255 \times 255$  by default and  $319 \times 319$  for NFS30, UAV123, and LaSOT. The  $\epsilon$  in Equation (8) is set to 0.01. The  $\sigma$  in Equation (9) is set to 0.0025.

## B. Faster Speed with Interpolation.

The successful application of deep networks [23] like ResNet-50 [14] is crucial on desirable performance of a tracker. Since the search region has generally the same resolution by rescaling the target from the original image, a modified ResNet with the stride of the downsampled convolution from the last two blocks changing from 2 to 1. To increase the receptive field, dilated convolutions with a rate 2 are applied. We instead propose to use the original ResNet. To ensure the same feature size for layerwise aggregation,

training data	VOT2018			NUO323	
	Acc	R	EAO	AUC	NPr
VYCLG	0.608	0.080	0.564	0.671	0.859
VYCD	0.602	0.089	0.539	0.664	0.856
VYC	0.604	0.103	0.530	0.661	0.846
VC	0.588	0.098	0.519	0.646	0.835

Table 11. Ablation study on the effect of training data.

we interpolate the features from the last two blocks to the same size of feature from block 2 (with stride 8). Compared with the original approach, the interpolation greatly saves the computation cost from the last two blocks since the input feature has a smaller spatial size due to downsampling. Compared with the baseline of SiamRPN++ operating at 46 FPS on an NVIDIA Titan Xp GPU, the offline classification module alone in our framework can operate at 90 FPS, achieving a 96% speed gain.

### C. Cumulative A and R on VOT2018

Since we follow the same post-processing process as [24], several hyper-parameters are introduced during tracking. We observe that A and R can vary drastically with different sets of hyper-parameters (i.e., window influence, penalty\_k, etc.). A model with a higher R will often yield a higher A (The accumulation error will be eliminated more often with more re-initialization). Therefore, the comparison can be substantially nullified if on a fixed set of hyper-parameters or their respective optimal set of hyper-parameters. To account for the problem and conduct a more trustworthy comparison, we report the average results of each model over multiple sets of hyper-parameters (140 in practice). We report the cumulative mean of A and R on these 140 runs. As shown in Figure 7, the averaged A and R are more stable for a stable comparison and analysis.

### D. Impact of Training Data

Our original tracker is trained using a collection of ImageNet VID (V) [35], Youtube-BB (Y) [33], COCO (C) [27], LaSOT (L) [8], and GOT-10k (G) [17]. The original full model is trained using VYCLG. For a more fair comparison with previous works [23], we train our tracker using VYCD. We also study the models with less data - VYC and VC. We evaluate the performance on VOT2018 and NUO323. Results are reported in Table 11. We can see that the performance of the model trained with VYCD only drops a little and still achieves state-of-the-art performance. The model trained with minimal data can still achieve an EAO of 0.520 on VOT2018 and an AUC of 0.646 on NUO323, demonstrating the strong generalization ability of our proposed method.

### E. Detailed Results

We provided the detailed results in figures on OTB2015 [42], NFS [20], UAV123 [29], and LaSOT [8] datasets, as shown in Figure 8. Our methods performs among the top methods for all the above datasets.

### F. Visualization of the Voted Boxes

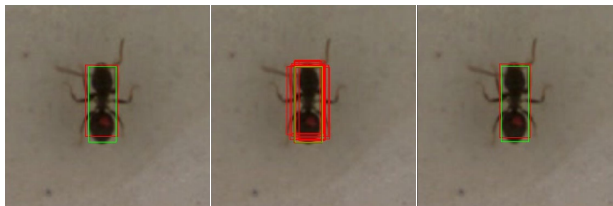


Figure 10. Visualization of proposed score voting strategy. Best viewed with color.

To demonstrate the effectiveness of our proposed score voting strategy, we give a visualized results of voted boxes, shown in Figure 10. Green denotes the groundtruth box and red denotes the predicted boxes. The bounding box from the leftmost figure is the predicted representation via direct regression. The middle figure showcases the chosen top-10 adjacent boxes according to their assigned voting weight. The final fused box representation is demonstrated in the rightmost figure. The box representation after score voting can approximate the groundtruth box more accurately, resulting in a more high-fidelity and precise representation of the target.

### G. Visualization of the Results

To validate the effectiveness of our proposed method, we showcase the visualized results on certain sequences from VOT2018 and OTB100. Our proposed method achieves a balance between robustness and accuracy. From the top 4 columns of the Figure 9, compared with SiamRPN++ [23], we observe that our method fairly tackles the problem of target drift and inherits a strong discriminative ability from robust localization. Compared with DiMP [2], our tracker can locate the target center better thus further yield a more accurate bounding box. From the last columns, Skating2-1 #212 and Bolt2 #94, we can see that DiMP tends to generate a larger bounding box when similar objects are present around the target. A contributing factor is that when the online module treats these adjacent pixels as positive samples, the target center may be shifted and the tracker tends to treat the cluster as the same object. Comparatively speaking, our tracker can locate the target center more precisely with accurate localization.

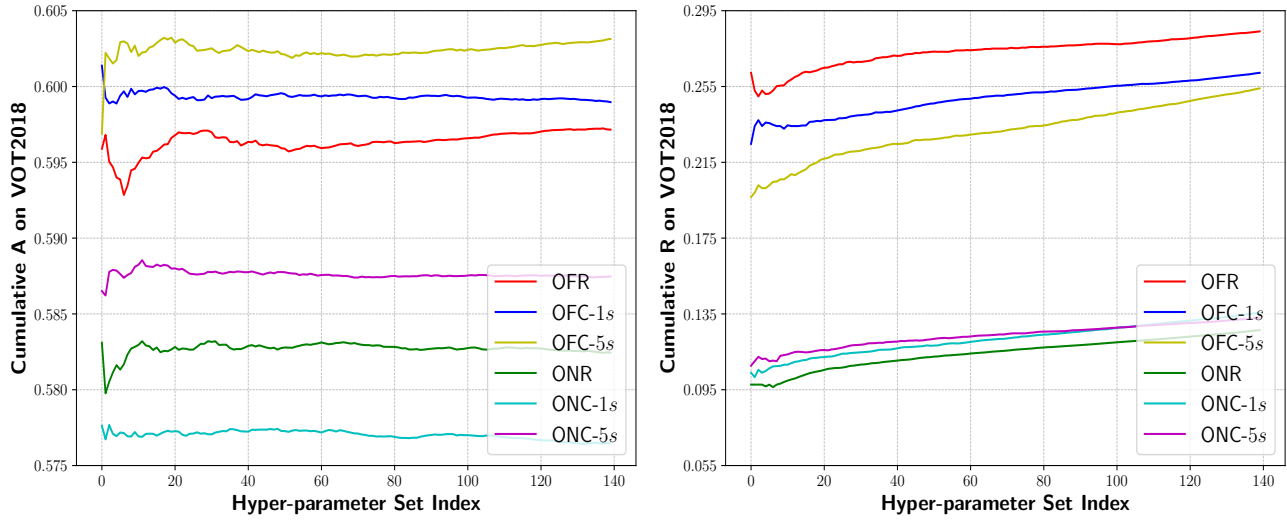


Figure 7. Cumulative average of Accuracy (left) and Robustness (right) on VOT2018.

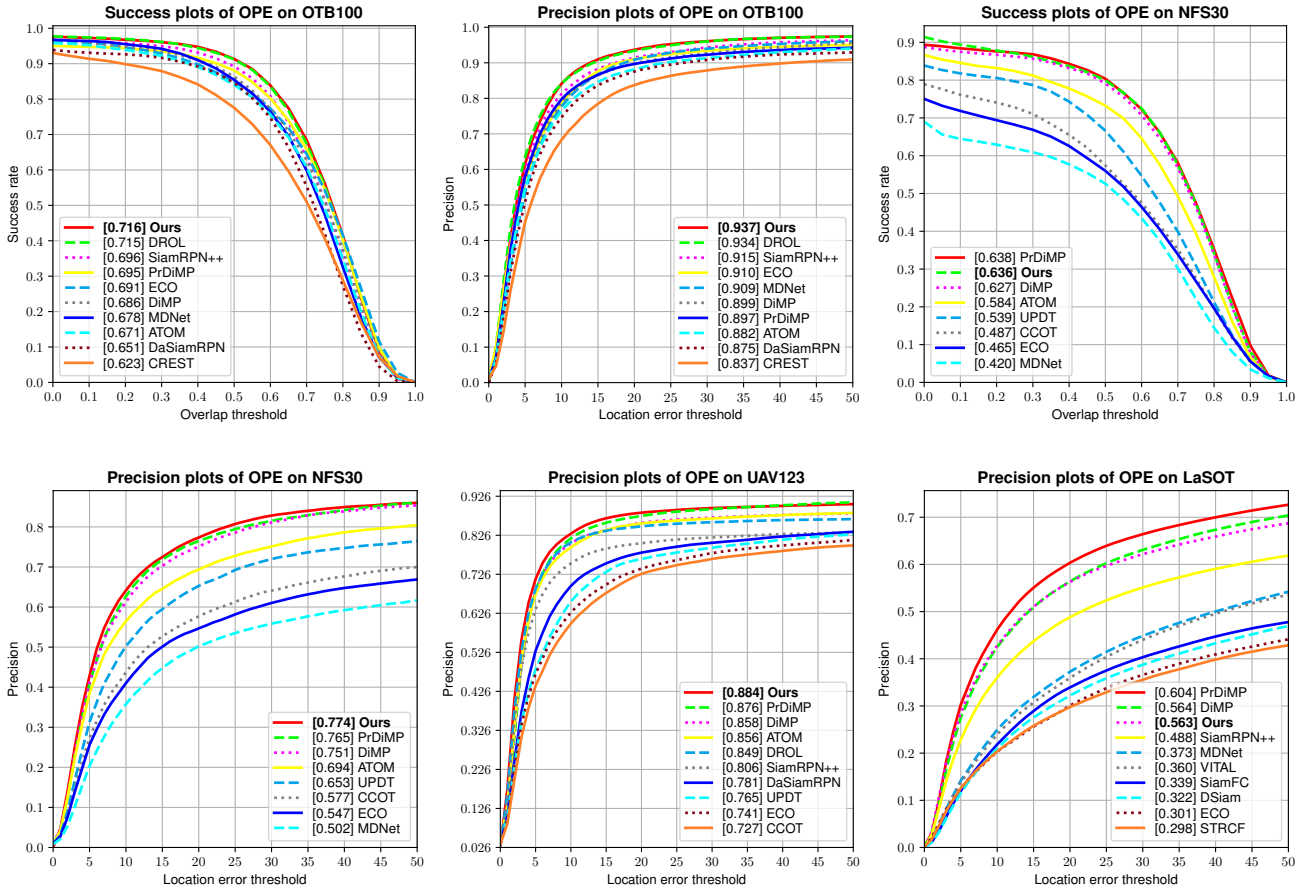
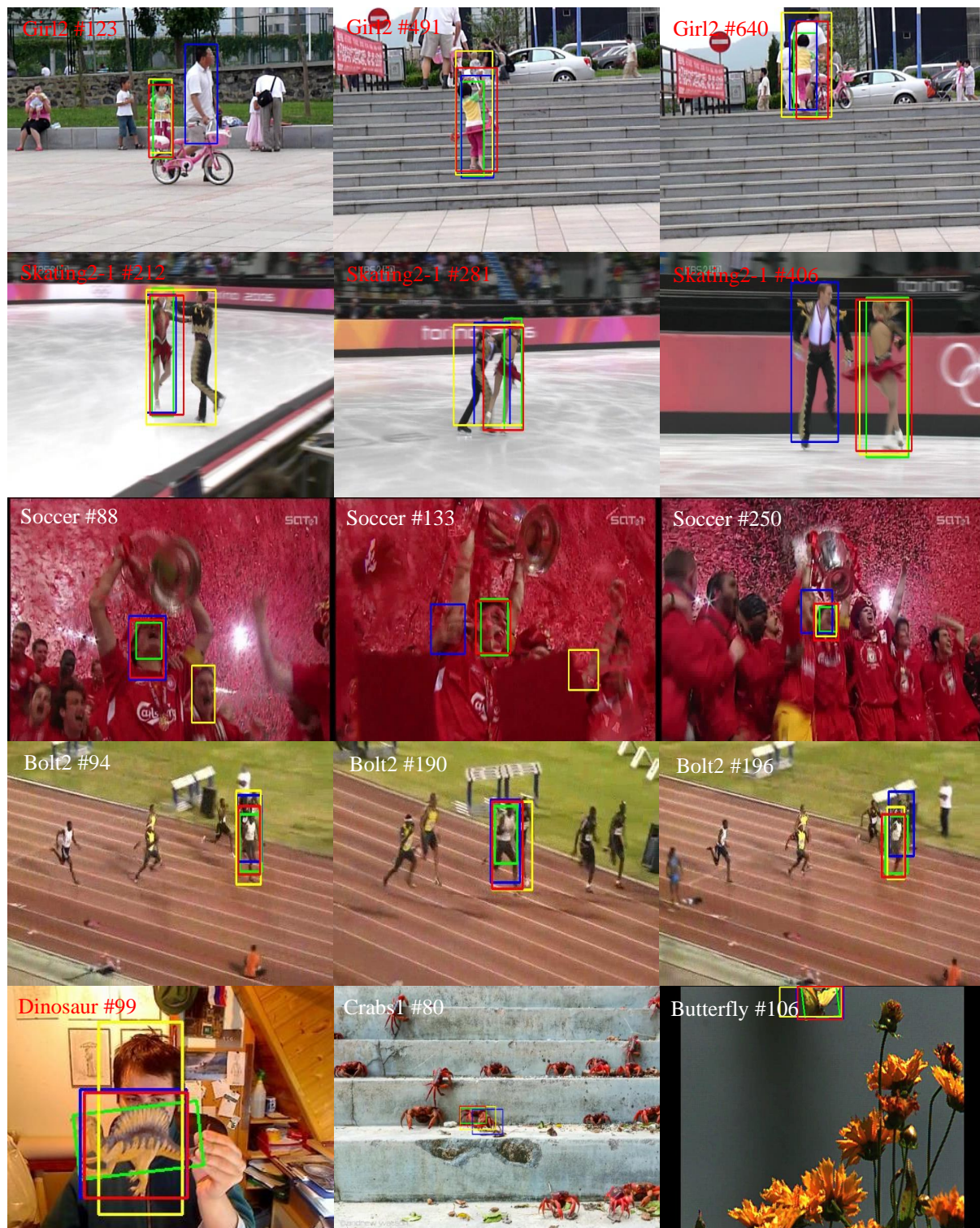


Figure 8. Results in terms of AUC and Precision score on OTB2015, NFS, UAV123 and LaSOT.



— Groundtruth — SiamRPN++ — DuML — Ours

Figure 9. Visualization of tracking results. Best viewed with color and zooming in.